Light-matter interactions in films of randomly distributed unidirectionally scattering dielectric nanoparticles

Parker R. Wray‡, and Harry A. Atwater, †,*

‡Department of Electrical Engineering, California Institute of Technology, Pasadena, CA 91125, USA

†Thomas J. Watson Laboratories of Applied Physics, California Institute of Technology, Pasadena, CA 91125, USA

1. Scattering amplitude coefficients for an isolated particle using Mie theory

For a single particle under plane wave illumination, there is no polarization conversion ($S_3 = S_4 = 0$) [1]. Using the notation from [1], with the origin being the center of the particle, the remaining two amplitude scattering elements can be written as an expansion

$$S_1 = \sum_{n=1}^{\infty} \frac{2n+1}{n(n+1)} (a_n \pi_n + b_n \tau_n) \ , \tag{10}$$

and

$$S_2 = \sum_{n=1}^{\infty} \frac{2n+1}{n(n+1)} (a_n \tau_n + b_n \pi_n) \ , \tag{11}$$

where $\tau_n = \frac{dP_n^1(\cos(\theta))}{d\theta}$ and $\pi_n = \frac{1}{sin\theta} P_n^1(\cos(\theta))$ are the angle-dependent basis functions, based on the associated Legendre polynomial (P_n^m) of order n and degree $m = 1$. The coefficients for this basis are a_n for transverse magnetic (TM) modes and b_n for transverse electric (TE) modes. The coefficients are found by applying the boundary conditions of field continuity between the particle and environment, leading to the well-known Mie solutions for non-magnetic particles

$$a_n = \frac{\eta \psi_n(\eta x) \psi_n'(x) - \psi_n(x) \psi_n'(\eta x)}{\eta \psi_n(\eta x) \xi_n'(x) - \xi_n(x) \psi_n'(\eta x)}, \tag{12}$$

and

$$b_n = \frac{\psi_n(\eta x) \psi_n'(x) - \eta \psi_n(x) \psi_n'(\eta x)}{\psi_n(\eta x) \xi_n'(x) - \eta \xi_n(x) \psi_n'(\eta x)}, \tag{13}$$

where $\psi_n(\rho) = \rho j_n(\rho)$ and $\xi_n(\rho) = \rho h_n^{(1)}(\rho)$ for $\rho \in \mathbb{C}$ [1]. The functions $j_n(\rho)$ and $h_n^{(1)}(\rho)$ are the spherical Bessel and Hankel functions of the first kind, respectively. The prime superscript denotes differentiation. The argument $x = \frac{2\pi r}{\lambda_0}$ is the size parameter from the main text. $\eta = n_s / n_e$ is the ratio of the complex refractive index of the particle (n_s) and environment (n_e). The scattering efficiency is written as,

$$\sigma_{sca} = \frac{2}{x^2} \sum_{n=1}^{\infty} (2n+1)(\|a_n\|^2 + \|b_n\|^2) \tag{14}$$

where we can decompose the scattering efficiency in to partial-efficiency terms for each mode as $\frac{1}{x^2} 2(2n+1)(\|a_n\|^2)$ and $\frac{1}{x^2} 2(2n+1)(\|b_n\|^2)$, which is the notation used in Figure 2b and 2e of the main text.

2. Scattering amplitude coefficients for a particle in a random film, using generalized Mie theory

Using the notation of [2] the amplitude scattering elements for generalized Mie theory are written as

$$S_1 = \sum_{n=1}^{\infty} \sum_{m=-n}^{n} \sum_{p=1}^{2} (-i)^n a_{mnp}^{\perp} \tau_{mn3-p}\,, \tag{15}$$

$$S_2 = \sum_{n=1}^{\infty} \sum_{m=-n}^{n} \sum_{p=1}^{2} (-i)^{n+1} a_{mnp}^{\parallel} \tau_{mnp}\,, \tag{16}$$

$$S_3 = \sum_{n=1}^{\infty} \sum_{m=-n}^{n} \sum_{p=1}^{2} (-i)^{n+1} a_{mnp}^{\perp} \tau_{mnp}\,, \tag{17}$$

and

$$S_4 = \sum_{n=1}^{\infty} \sum_{m=-n}^{n} \sum_{p=1}^{2} (-i)^{n} a_{mnp}^{\parallel} \tau_{mn3-p}\,, \tag{18}$$

where $a_{mnp}^{(s)}$ are the scattering coefficients for the TM $(p = 2)$ and TE $(p = 1)$ modes of degree m and order n. The superscript (s) denotes the state of incident polarization, either parallel ($\parallel$) or perpendicular ($\perp$) to the scattering plane.

The angular basis functions now account for non-unitary degree, $\tau_{mn2} = \tau_{mn} = C_{mn} \frac{dP_n^m(\cos(\theta))}{d\theta}$ and $\tau_{mn1} = \pi_{mn} = C_{mn} \frac{m}{sin\theta} P_n^m(\cos(\theta))$ where $C_{mn} = \sqrt{\frac{(2n+1)}{n(n+1)} \frac{(n-m)!}{(n+m)!}}$ is used for normalization. It is necessary to differentiate coefficients based on the incident polarization since the scattering object (i.e., the random nanoparticle array) no longer has rotation symmetry, in general. Similar to the single particle case, the scattering coefficients are found by applying the continuity equations, now accounting for interparticle coupling through application of the vector addition theorem [2]. The effect of particle placement and subsequent particle coupling is therefore encapsulated in the scattering coefficients of equations (15) - (18) [2]. We rewrite equations $(15) - (18)$ to a form more similar to the isolated Mie case directly from the property that

$$P_n^{-m}(cos\theta) = (-1)^m \frac{(n-m)!}{(n+m)!} P_n^m(cos\theta). \tag{19}$$

Therefore

$$\tau_{-mn1} = (-1)^m \frac{(n-m)!}{(n+m)!} \sqrt{\frac{(2n+1)}{n(n+1)} \frac{(n+m)!}{(n-m)!}} \frac{dP_n^m(cos\theta)}{d\theta} = (-1)^m \tau_{mn1} \tag{20}$$

and

$$\tau_{-mn2} = (-1)^m \frac{(n-m)!}{(n+m)!}\sqrt{\frac{(2n+1)}{n(n+1)}\frac{(n+m)!}{(n-m)!}}\frac{-mP_n^m(cos\theta)}{sin\theta} = (-1)^{m+1}\tau_{mn2}. \tag{21}$$

The resulting scattering amplitude elements are now

$$S_1 = \sum_{n=1}^{\infty}\sum_{m=0}^{n} f_m[A_{nm}^{\perp}\pi_{mn} + B_{nm}^{\perp}\tau_{mn}], \tag{22}$$

$$S_2 = \sum_{n=1}^{\infty}\sum_{m=0}^{n} f_m[A_{nm}^{\parallel}\tau_{mn} + B_{nm}^{\parallel}\pi_{mn}], \tag{23}$$

$$S_3 = \sum_{n=1}^{\infty}\sum_{m=0}^{n} f_m\left[A^{\times\perp}{}_{nm}\tau_{mn} + B^{\times\perp}{}_{nm}\pi_{mn}\right], \tag{24}$$

and

$$S_4 = \sum_{n=1}^{\infty}\sum_{m=0}^{n} f_m\left[A^{\times\parallel}{}_{nm}\pi_{mn} + B^{\times\parallel}{}_{nm}\tau_{mn}\right], \tag{25}$$

where

$$A_{nm}^{(s)} = \begin{cases}(-i)^{n+1}(a_{mn}^{\parallel} + (-1)^m a_{-mn}^{\parallel}), & (s) = \parallel \\ (-i)^n(a_{mn}^{\perp} + (-1)^{m+1}a_{-mn}^{\perp}), & (s) = \perp\end{cases}, \quad B_{nm}^{(s)} = \begin{cases}(-i)^{n+1}(b_{mn}^{\parallel} + (-1)^{m+1}b_{-mn}^{\parallel}), & (s) = \parallel \\ (-i)^n(b_{mn}^{\perp} + (-1)^m b_{-mn}^{\perp}), & (s) = \perp\end{cases},$$

$$A^{\times(s)}{}_{nm} = \begin{cases}(-i)^n(a_{mn}^{\parallel} + (-1)^{m+1}a_{-mn}^{\parallel}), & (s) = \parallel \\ (-i)^{n+1}(a_{mn}^{\perp} + (-1)^m a_{-mn}^{\perp}), & (s) = \perp\end{cases}, \quad B^{\times(s)}{}_{nm} = \begin{cases}(-i)^n(b_{mn}^{\parallel} + (-1)^m b_{-mn}^{\parallel}), & (s) = \parallel \\ (-i)^{n+1}(b_{mn}^{\perp} + (-1)^{m+1}b_{-mn}^{\perp}), & (s) = \perp\end{cases}, \tag{26}$$

which more closely resembles the isolate Mie solution from section 1 of the supplementary information. $f_m = \frac{1}{1+\delta(m)}$ is to ensure the $m = 0$ case is not overcounted. Removing the negligible terms and incorporating all relevant simplifications detailed in the second section of the main text, the average angle resolved scattering efficiency for the observation particle can be written as

$$\begin{aligned} E[Q_s^{\parallel}(\theta)] &= \frac{1}{x^2}(E[\|S_2\|^2] + E[\|S_3\|^2]) \\ &= \frac{1}{x^2}E\left[\left(\left\|A_{11}^{\parallel}\right\|^2 + \left\|A^{\times\perp}{}_{11}\right\|^2\right)\tau_{11}^2 + \left(\left\|B_{11}^{\parallel}\right\|^2 + \left\|B^{\times\perp}{}_{11}\right\|^2\right)\pi_{11}^2 + \left(A_{11}^{\parallel}B_{11}^{\parallel *} + A_{11}^{\parallel *}B_{11}^{\parallel}\right)\tau_{11}\pi_{11}\right] \end{aligned} \tag{28}$$

$$E[Q_s^{\perp}(\theta)] = \frac{1}{x^2}(E[\|S_4\|^2] + E[\|S_1\|^2])$$
$$= \frac{1}{x^2}E\left[\left(\|B_{11}^{\perp}\|^2 + \left\|B^{\times\parallel}{}_{11}\right\|^2\right)\tau_{11}^2 + (\|A_{11}^{\perp}\|^2 + \left\|A^{\times\parallel}{}_{11}\right\|^2)\pi_{11}^2 + (A_{11}^{\perp}B_{11}^{\perp *} + A_{11}^{\perp *}B_{11}^{\perp})\tau_{11}\pi_{11}\right]. \quad (29)$$

We can further simplify equations (28) and (29), with respect to the average response, by recognizing that the set of particle distributions for the different incident polarization states can be made the same through rotating each particle distribution by 90 degrees. Formally this is equivalent to stating

$$\Delta_{11}^{\parallel(j)} = \Delta_{11}^{\perp(k)} \rightarrow \Delta = \{\Delta_{11}^{\parallel(j)}, \Delta_{11}^{\perp(k)}\} \quad (30)$$

where $\Delta = \mathrm{A}, \mathrm{B}, \mathrm{A}^{\times}, B^{\times}$ and the superscript (j) denotes the j^{th} distribution of particles and (k) is the j^{th} distribution rotated by 90 degrees. Adding the rotated sets, we can remove the difference between parallel and perpendicular coefficients (i.e., the (s) superscript), in the average sense, resulting in the satisfying final form of equations (6) and (7) from the main text.

3. Particle and cluster level cross sections using generalized Mie theory

From the viewpoint of a single particle in a random particle film, both the incident and multiply scattered field are considered part of the field that excites the particle. Therefore, we can write the energy balance for particle j inside a cluster of N particles in terms of a total excitation field, written as $C_{exc,j} = C_{sca-i,j} + C_{abs,j} = C_{ext,j} - C_{sca-d,j}$. In this formula, $C_{abs,j}$ is the particle absorption cross section and $C_{sca-i,j}$ is the particle's independent scattering cross section [2]. The first equality provides a result similar to traditional Mie theory, $C_{exc,j} = C_{sca-i,j} + C_{abs,j}$, where all cross sections are positive. The second equality, $C_{exc,j} = C_{ext,j} - C_{sca-d,j}$, shows that the excitation cross section can be view as the interference from the particle's scattered field with the incident field and the multiply scattered field [2]. The dependent scattering cross section, $C_{sca-d,j}$, describes the power flowing to or from the sphere as a result of the sphere's scattered field interacting with the multiply scattered field [2]. The particle level extinction cross section, $C_{ext,j}$, describes the interaction with the incident plane wave [2]. It is important to note that $C_{ext,j} \neq C_{sca-i,j} + C_{abs,j}$, unless $C_{sca-d,j} = 0$, which is the special case associated with isolated Mie theory. Furthermore, it is not necessary that $C_{ext,j} > C_{abs,j}$ or that $C_{ext,j} > 0$ [2]. For passive particles, both $C_{sca-i,j}$ and $C_{abs,j}$ are positive [2]. Both $C_{ext,j}$ and $C_{sca-d,j}$ can be positive or negative, but they will sum to a positive number. Particle level efficiencies are then defined by division of the cross section by the particle's cross-sectional area, $\sigma_j = C_j/\pi r_j^2$.

We can write the average particle level independent scattering efficiency for the sampled particles in a random particle film as

$$E[\sigma_{sca-i}] = \frac{2}{x^2}\sum_{n=1}^{\infty}\sum_{m=0}^{n} E\left[\left\|A_{nm,j}\right\|^2 + \left\|B_{nm,j}\right\|^2 + \left\|A^{\times}_{nm,j}\right\|^2 + \left\|B^{\times}_{nm,j}\right\|^2\right] \tag{31}$$

where polarization dependence is removed by incorporating particle distributions with 90-degree rotations, as outlined in section 2 of the supplementary information. The mode decomposed independent scattering efficiency terms are written as $\frac{2}{x^2}E\left[\left\|\Delta_{nm,j}\right\|^2\right]$, where $\Delta = \mathrm{A}, \mathrm{B}, \mathrm{A}^{\times}$, or $B^{\times}$. This is the notation used to plot the efficiency of scattering coefficients in Figure 3 of the main text.

The total extinction, absorption, and scattering cross sections of the particle cluster can be found by,

$$\sum_{j=1}^{N} C_{ext,j} = C_{ext}, \tag{32}$$

$$\sum_{j=1}^{N} C_{abs,j} = C_{abs}, \tag{33}$$

and

$$\sum_{j=1}^{N} C_{sca-i,j} + C_{sca-d,j} = C_{ext} - C_{abs} = C_{sca}, \tag{34}$$

where the summation is done over the N particles in the cluster and removal of the j subscript indicates the total cluster cross section. The cluster level cross sections obeys the energy balance equation $C_{ext} = C_{abs} + C_{sca}$ [2]. In this case, the particle cluster is now viewed as a singular scattering object. The multiply scattered field is considered part of the total scattered field and we are interested in the energy removed from the incident field by the entire particle cluster.

4. Estimating the reflection, transmission, and absorption of a film of randomly distributed Kerker particles

From the viewpoint of photon counting, we can define the per unit area absorbed (Abs) and scattered (Sca) energy resulting from a wave impinging on an infinite particle film of identical particles as,

$$Abs = \frac{\mathrm{C_{abs}}}{\mathrm{A}} = \frac{ff}{\pi r^2} \lim_{N\to\infty} \frac{1}{N} \sum_{j=1}^{N} C_{abs,j} = ffE[\sigma_{abs}] \tag{35}$$

and

$$Sca = \frac{\mathrm{C_{sca}}}{\mathrm{A}} = \frac{ff}{\pi r^2} \lim_{N\to\infty} \frac{1}{N} \sum_{j=1}^{N} C_{sca-i,j} + C_{sca-d,j} = ffE[\sigma_{sca}] \tag{36}$$

where A is the film area (infinite), $ff = N\pi r^2/A$ is the particle fill fraction, and r is the particle radius. This result comes directly from the definition of the cluster level cross sections and particle level efficiency, which is detailed in section 3 of the supplementary information. From the first equality in equations 35 and 36 we find that the film's per unit area absorbed and scattered energy are functions of the expected value of the particle level absorption and total scattering cross section ($C_{sca,j} = C_{sca-i,j} + C_{sca-d,j}$). The last equality in equations 35 and 36 show that the film level absorption and scattering can be written in terms of particle level efficiencies, where $\sigma_j = \mathrm{C_j}/\pi \mathrm{r_j^2}$ for particle j [2]. Therefore, we can estimate the absorbed and scattered energy by summing over a critical number of randomly sampled particles ($N_c = 100$ in our study), where convergence of the statistical average to the true expected value is guaranteed by the law of large numbers. We simulate the process of sampling particles in an infinite particle film by sampling the center particle (termed the observation particle in the main text) in a finite sized but sufficiently large random particle film. Within the finite sized particle film, all particle coupling effects are being accounted for through the use of generalized Mie theory. Given that there is no long range order, the potential contribution of coupling effects on the observation particle by particles beyond the finite simulation size is being regarded as negligible. Then, according to [1], we can approximate the efficiency of photons scattered in the reflection ($Sca_{backward}$) and transmission ($Sca_{forward}$) direction as

$$Sca_{forward} = ff \lim_{N\to\infty} \frac{1}{N} \sum_{j=1}^{N} Q_{s,j}(\theta = 0°) = ff\, E[\mathrm{Q_s}(\theta = 0°)] \tag{37}$$

and

$$Sca_{backward} = ff \lim_{N\to\infty} \frac{1}{N} \sum_{j=1}^{N} Q_{s,j}(\theta = 180°) = ff\ E[\mathrm{Q_s}(\theta = 180°)] \quad (38)$$

where Q_s is the angle resolved scattering efficiency function described in equations 4 and 5 of the main text. In this formula we remove the need to account for the dependence on incident polarization states by summing particle distributions and their 90 degree rotation, as outlined in section 2 of the supplementary information. We can then define the film level forward-to-backward ratio, denoted as the FBR_A in the main text, as $Sca_{forward}/Sca_{backward} = E[Q_s(\theta = 0)]/E[Q_s(\theta = 180)]$. For the particles we are studying, the solution to $E[\mathrm{Q_s}(\theta)]$ is found to maintain Kerker behavior and is given by equations 6 and 7 in the main text.

Therefore, for an infinite particle film of monolayer thickness, we write the absorption as $Abs = ffE[\sigma_{abs}]$. The fraction of photons elastically scattered in an infinite particle film of monolayer thickness is written as $Sca = ffE[\sigma_{sca}] \approx Sca_{backward} + Sca_{forward}$. The reflection from the infinite particle film is then defined as $Ref = Sca_{backward} = ffE[\sigma_{sca,i}]/(1 + FBR_A)$, by direct substitution of $Sca = (1 + FBR_A)Sca_{backward}$. The transmission is found through energy conservation $Tran + Ref + Abs = 1$.

5. Supplementary figures

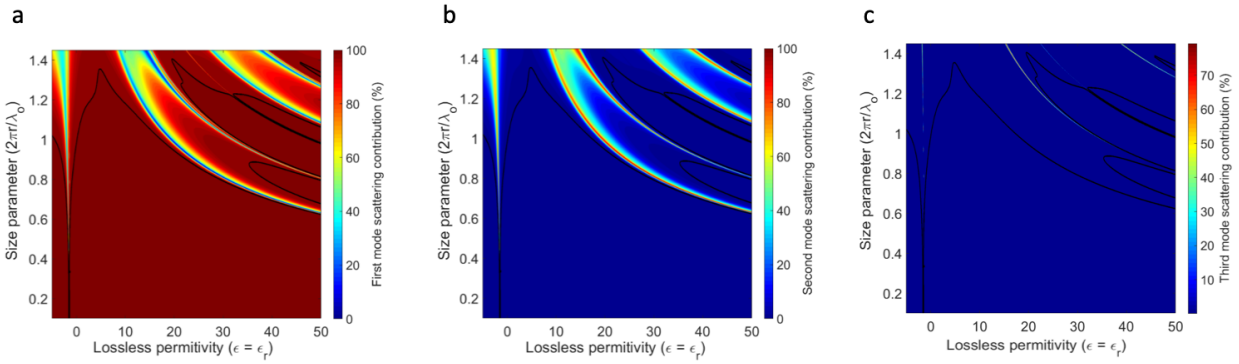

Figure S1. Mode contribution to the total scattering cross section for a single lossless nanoparticle. (a) Normalized contribution of the first order modes to the total scattering cross section. (b) Normalized contribution of the second order modes to the total scattering cross section. (c) Normalized contribution of the third order modes to the total scattering cross section. All graphs were calculated using Mie theory, up to fifth order modes. No non-zero mode contributions were found for modes above the third order.

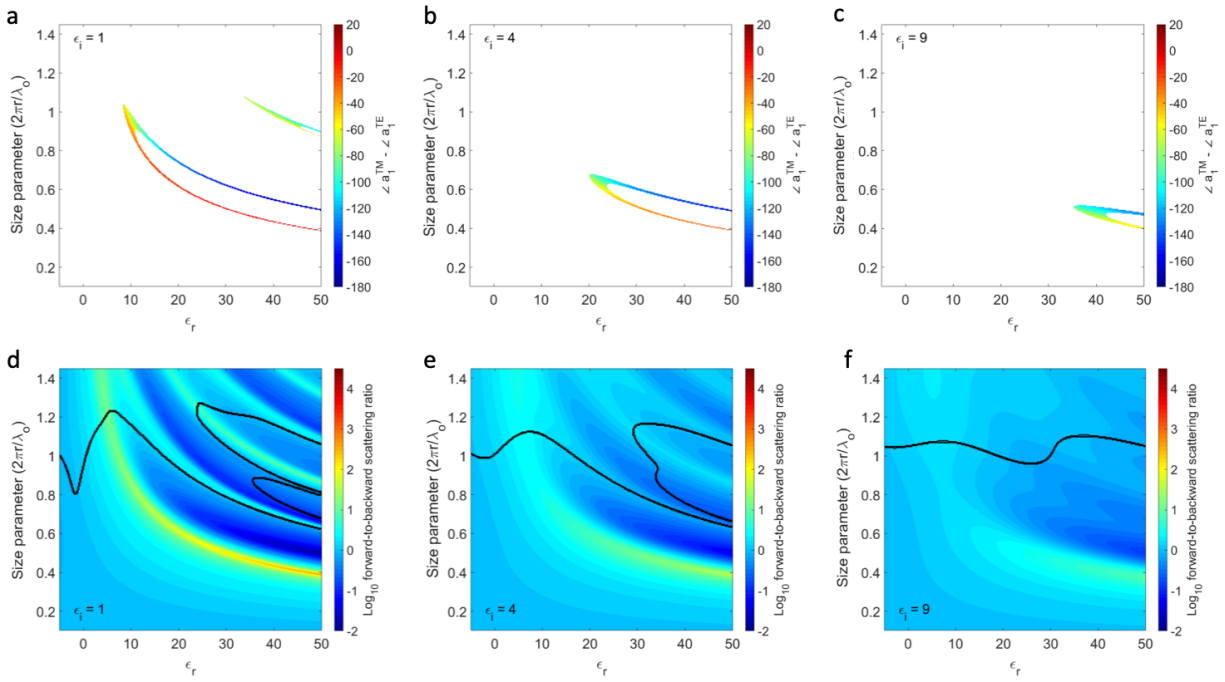

Figure S2. Effect of material loss on satisfying polarization invariance Kerker condition, and forward-to-backward ratios. Figure S2a-c shows the phase difference between the first order TM and TE modes, in the regime where the normalized difference in the mode magnitudes is less than one tenth. Figure S2a-c are plotted for imaginary permittivity equal to one, four, and nine, respectively. Figure S2d-f, shows the corresponding log base ten forward-to-backward scattering ratios, with a black line overlay showing the cutoff when the first order modes contribute less than ninety nine percent of the scattering cross section.

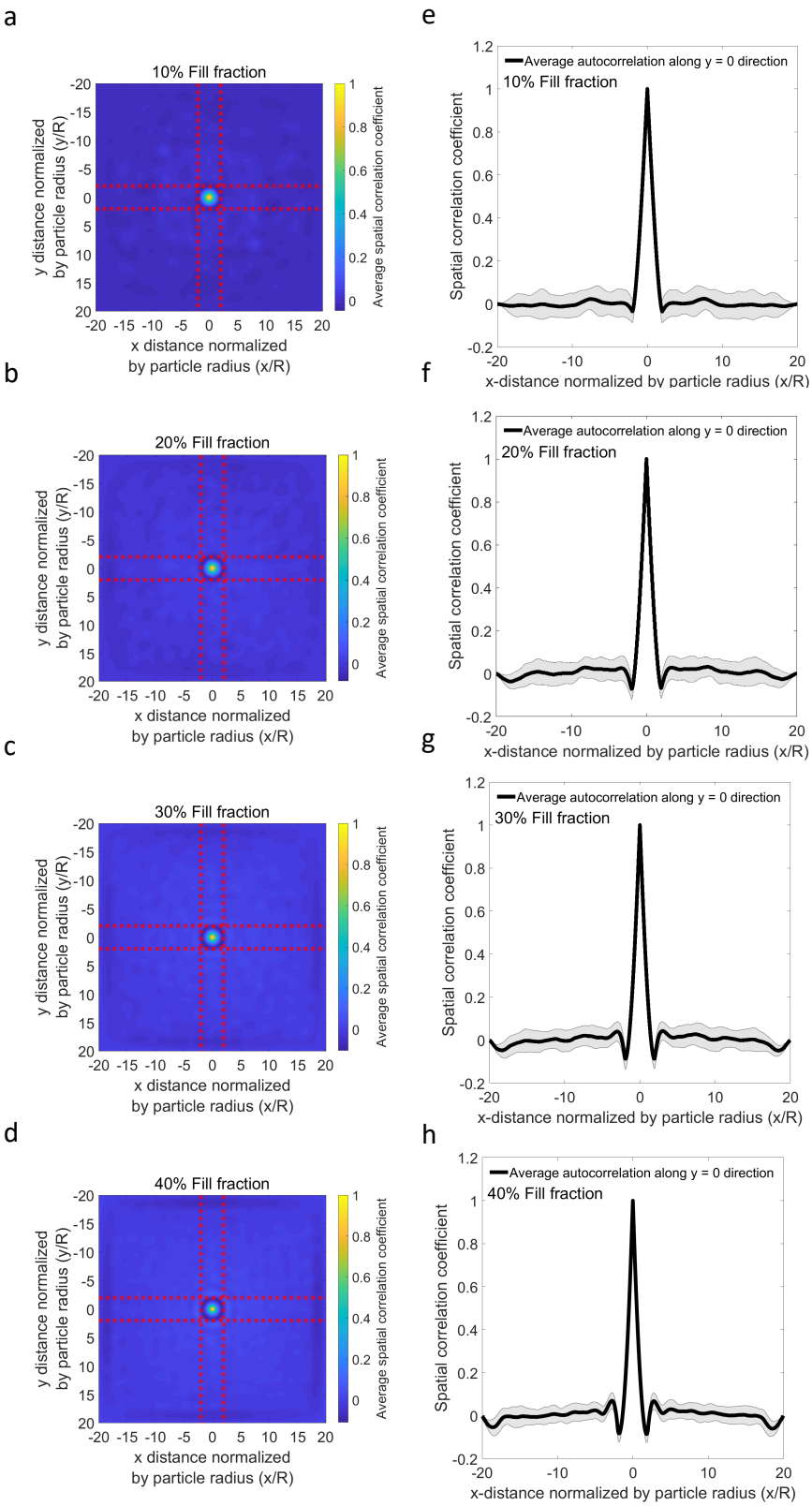

Figure S3. Average spatial autocorrelation functions of the 50 unique particle distributions and their 90 degree rotations for Si, used in section 3. (a-d) Average spatial autocorrelation function for 88nm diameter Si particles randomly distributed with fill fractions of (a) 10%, (b) 20%, (c) 30%, and (d) 40%. (e-h) Line profile of the autocorrelation along the y = 0 direction. The solid black line represents the average autocorrelation. The shaded area is one standard deviation from the average.

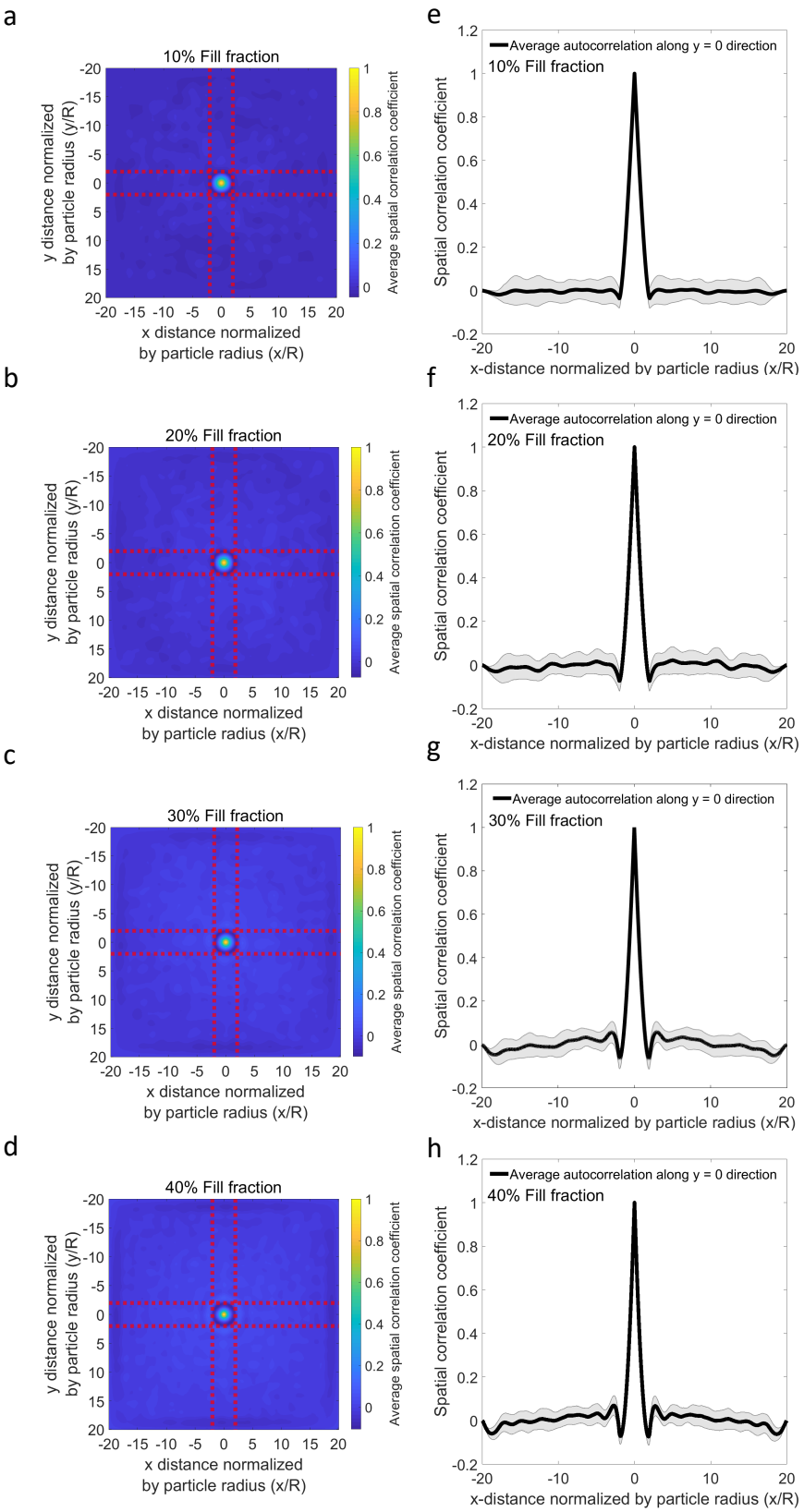

Figure S4. Average spatial autocorrelation functions of the 50 unique particle distributions and their 90 degree rotations for GaN, used in section 3. (a-d) Average spatial autocorrelation function for 280nm diameter GaN particles randomly distributed with fill fractions of (a) 10%, (b) 20%, (c) 30%, and (d) 40%. (e-h) Line profile of the autocorrelation along the y = 0 direction. The solid black line represents the average autocorrelation. The shaded area is one standard deviation from the average.

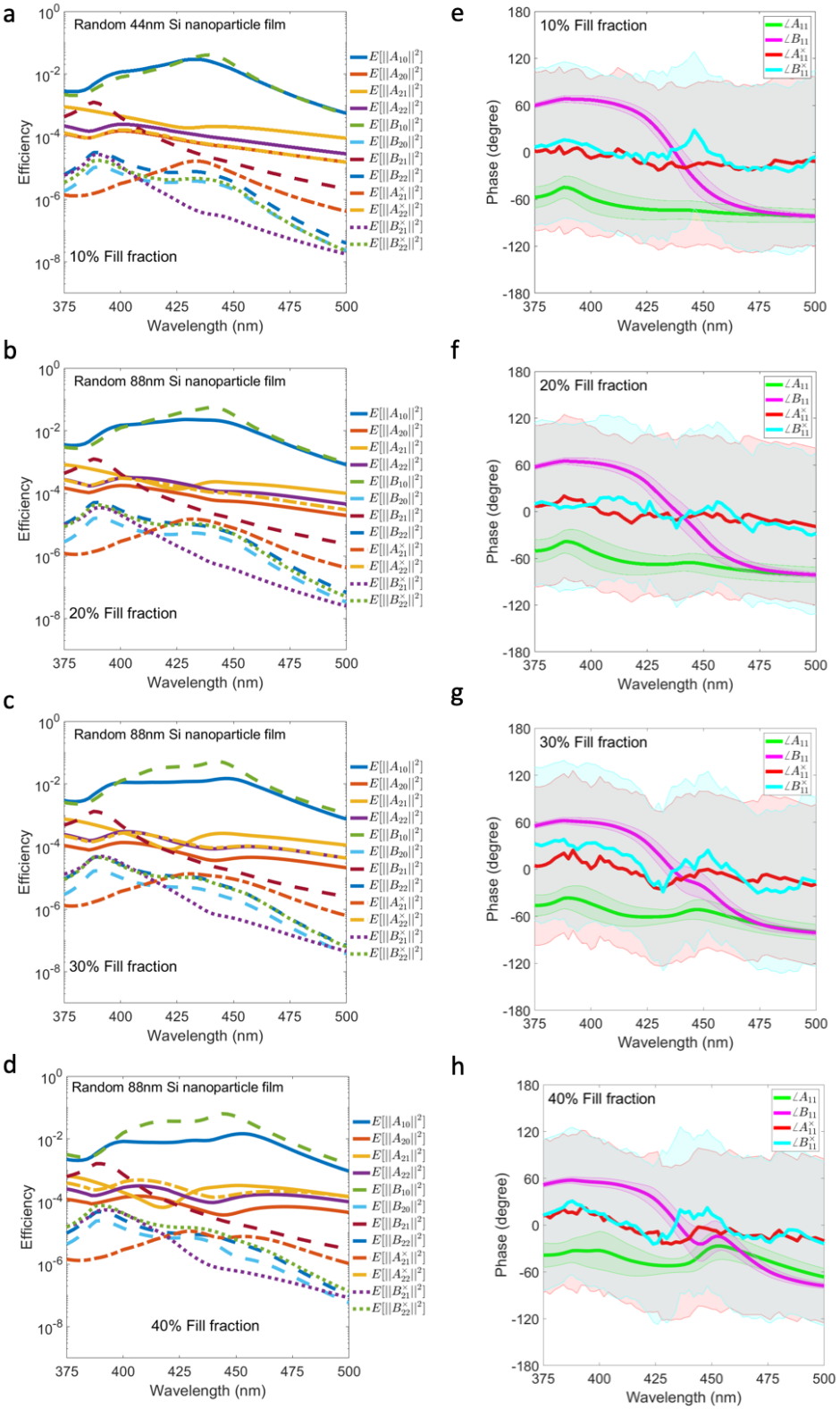

Figure S5. Contribution of higher order modes to the scattering response and the phase profiles of the dominant scattering modes for an 88nm Si particle embedded in a random Kerker film of 88nm Si particles. (a-d) Average contribution of the $mn = \{01,02,12,22\}$ modes to the independent scattering cross-section for fill fractions of (a) 10%, (b) 20%, (c) 30%, and (d) 40%. (e-h) Phase profile of the dominant scattering modes $mn = \{11\}$, showing the cross-polarization terms have random phase for (e) 10%, (f) 20%, (g) 30%, and (h) 40% fill fraction. The solid lines represent the average response and the corresponding shaded area is the area within one standard deviation of the mean. Statistics were based on 50 unique particle distributions and their 90-degree rotations (100 simulations in total)

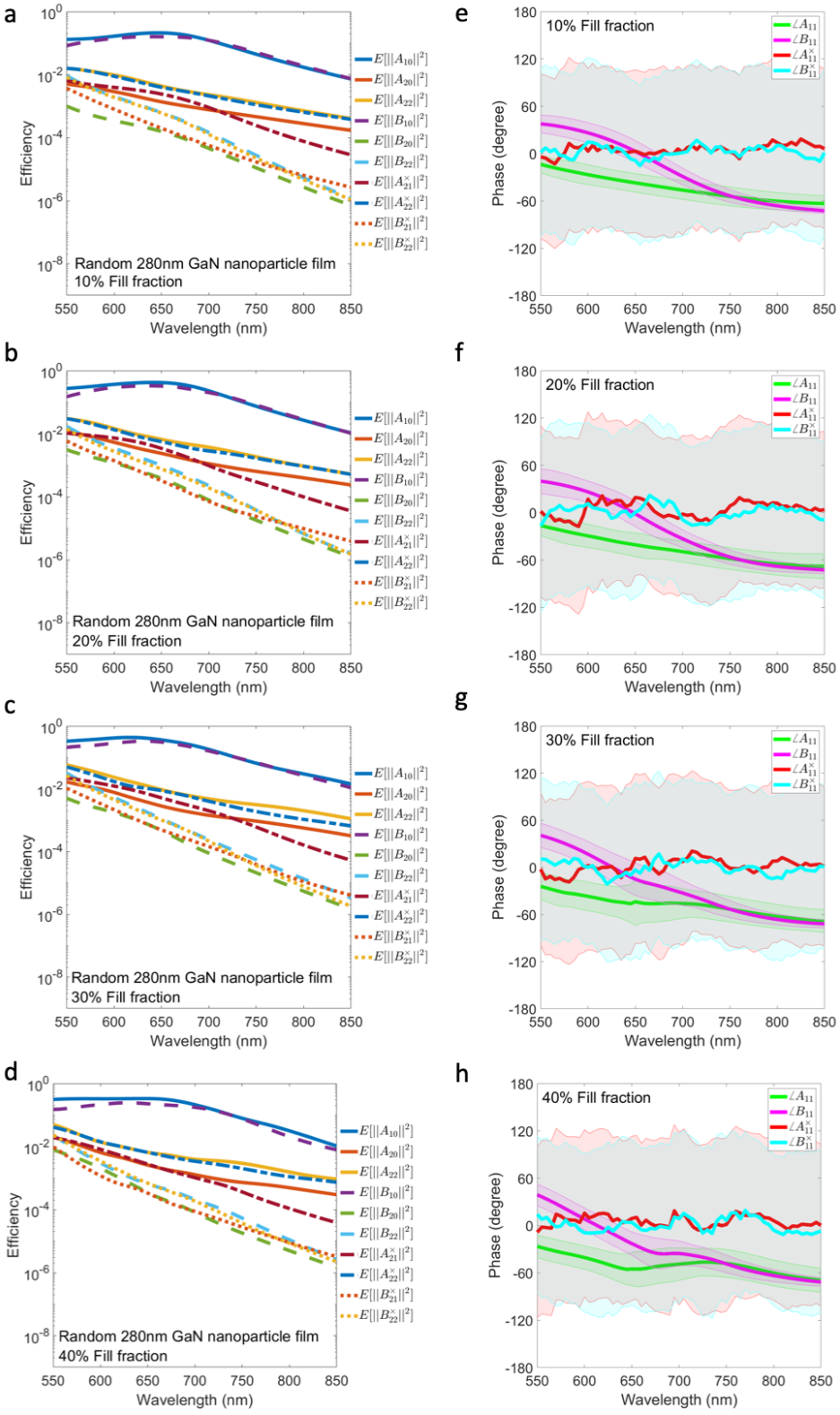

Figure S6. Contribution of higher order modes to the scattering response and the phase profiles of the dominant scattering modes for an 280nm GaN particle embedded in a random Kerker film of 280nm GaN particles. (a-d) Average contribution of the $mn = \{01,02,12,22\}$ modes to the independent scattering cross-section for fill fractions of (a) 10%, (b) 20%, (c) 30%, and (d) 40%. (e-h) Phase profile of the dominant scattering modes $mn = \{11\}$, showing the cross-polarization terms have random phase for (e) 10%, (f) 20%, (g) 30%, and (h) 40% fill fraction. The solid lines represent the average response and the corresponding shaded area is the area within one standard deviation of the mean. Statistics were based on 50 unique particle distributions and their 90-degree rotations (100 simulations in total).

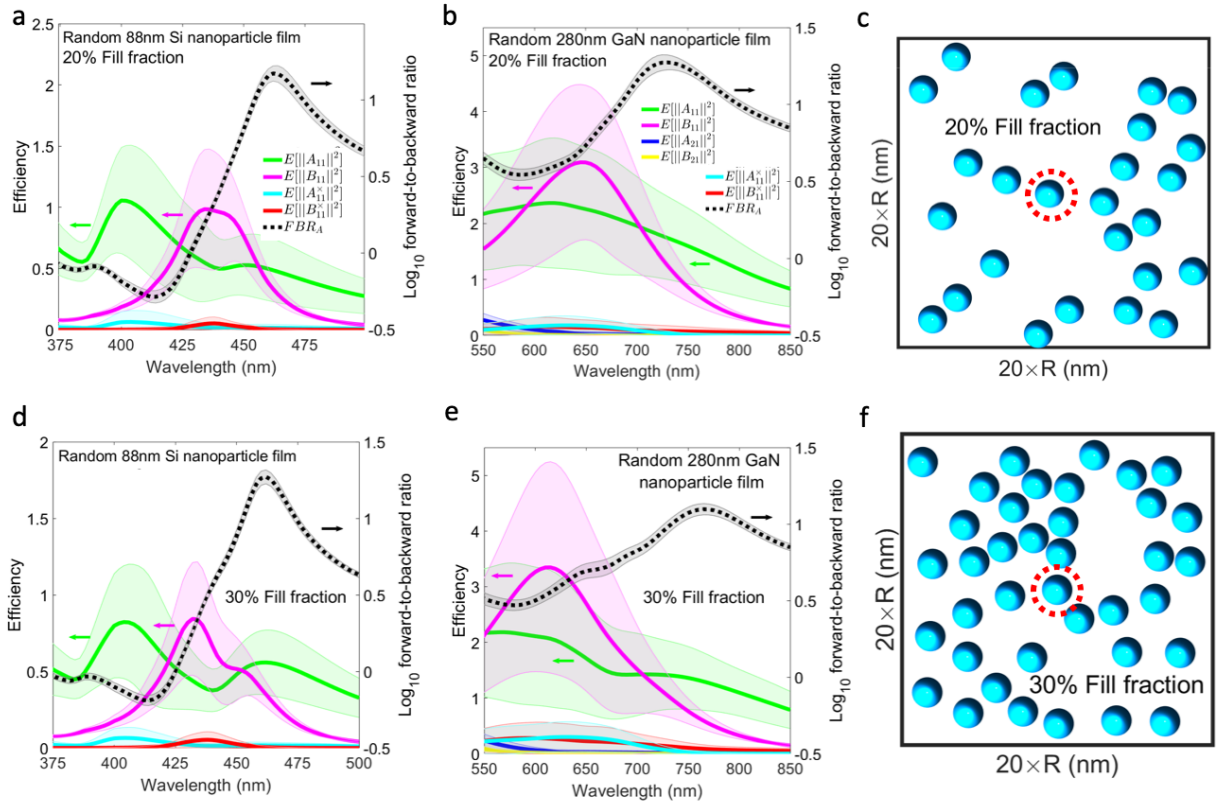

Figure S7. Scattering behavior of Kerker particles embedded in a random monolayer Kerker particle film. (a,d) Efficiency scaled magnitude of the dominant scattering modes and FBR_A for an 88 nm diameter Si particle embedded in a random particle film with fill fractions of (a) 20% and (d) 30%. (c,e) Corresponding results for 280 nm diameter GaN particle embedded in a random particle film with fill fractions of (b) 20% and (e) 30%. (c,f) Top-view graphical representation of a random particle film with fill fractions of (c) 20%, and (f) 30%. The red dashed circle outlines the observation particle. The length and width of the film are given as a function of particle radius (R). The solid color lines show the average (N=100) mode contribution to the independent scattering efficiency (left y-axis). The corresponding shaded area is the area one standard deviation from the mean. The dashed black line shows the FBR_A for the average scattering response (right y-axis).

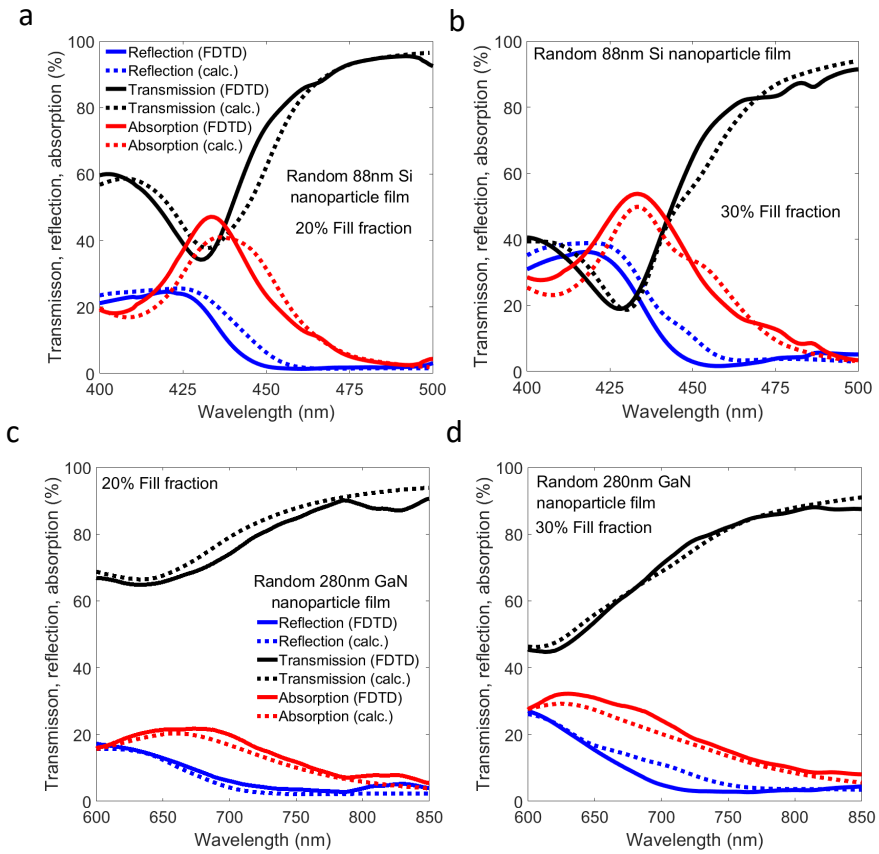

Figure S8. Comparison of the reflection, transmission, and absorption (RTA) in random monolayer Kerker films at normal incidence. In all cases the solid lines are the average FDTD-based RTA response, taken from Figure 4, and the dashed lines are the average RTA response predicted from equation (8) using the data from section 2 in the main text. (a,b) RTA of 88 nm diameter Si random particle films for (a) 20% and (b) 30% fill fraction. (c,d) RTA of the 280 nm diameter GaN random particle films for (c) 20% and (d) 30% fill fraction.

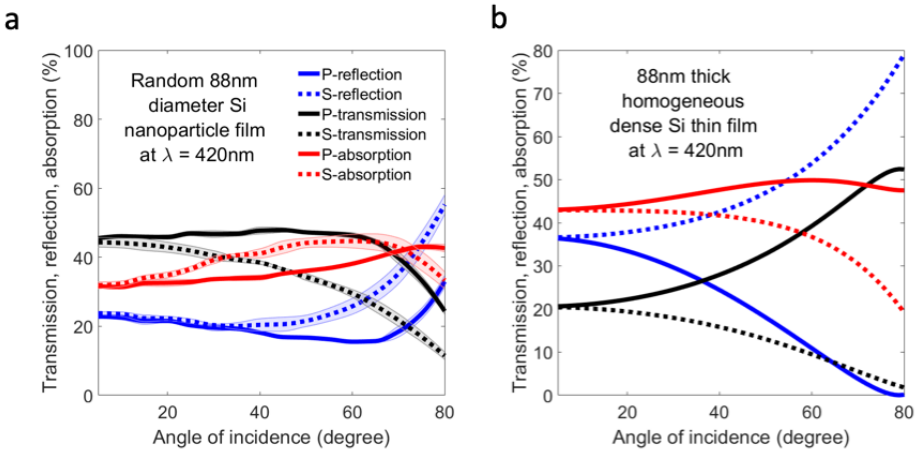

Figure S9. Angular response of random Kerker films with a fill fraction of 20%. (a) RTA for randomly placed 88 nm Si particles as a function of angle, at a wavelength of 420 nm (backward-Kerker regime). (b) Corresponding RTA angular response for an 88 nm Si slab at a wavelength of 420 nm.

References

1. C. F. Bohren and D. R. Huffman, Absorption and Scattering of Light by Small Particles (Wiley-VCH, 2004).

2. D. W. Mackowski and M. I. Mishchenko, "A multiple sphere T-matrix Fortran code for use on parallel computer clusters," Journal of Quantitative Spectroscopy and Radiative Transfer 112, 2182–2192 (2011).